List of publications

1. S.N. Aideo, D. Mohanta, Limiting hydrophobic behavior and reflectance response of dragonfly and damselfly wings, *Applied surface science*, 387(3), 2016, 609.

2. S.N. Aideo, D. Mohanta , Surface-wettability and Structural Colouration Property of Certain *Rosaceae* Cultivars with Off-to-dark Pink appearances, *Journal of Bionic Engineering* 15 (6), 1012-1024, 2018.

3. S.N. Aideo, D. Mohanta, Origin of white-appearing structural coloration in the wings of butterflies belonging to *Lepidoptera* order but diverse sub-families, *Journal of Applied Physics* (under review).

Other publications

1. Swati N. Aideo, Dambarudhar Mohanta, *Journal of Physics: Conference Series* 765 (2016) 012019.
2. Swati N. Aideo, Rajib Haloi and Dambarudhar Mohanta, "Exploring structural colour in uni- and multi-coloured butterfly wings and Ag^{+} uptake by scales", *EPL*, 119 (2017) 66003.

Applied Surface Science 387 (2016) 609–616

Contents lists available at ScienceDirect

Applied Surface Science

journal homepage: www.elsevier.com/locate/apsusc

Limiting hydrophobic behavior and reflectance response of dragonfly and damselfly wings

Swati Nawami Aideo, Dambarudhar Mohanta*

Nanoscience and Soft Matter Laboratory, Department of Physics, Tezpur University, Napaam, Tezpur, Assam 784 028, India

ARTICLE INFO

Article history:
Received 9 December 2015
Received in revised form 26 May 2016
Accepted 9 June 2016
Available online 14 June 2016

PACS:
68.08.Bc
68.08.De
68.35.Ct
78.40.Pg
87.64.-t

Keywords:
Surface roughness
Contact angle
Hydrophobic
Dewetting
Chitin

ABSTRACT

In this work, through water contact angle (CA) measurements, we explore hydrophobic behavior of different parts of the hind wings of a dragonfly, *Gynacantha Dravida* and of a damselfly, *Pseudagrion Microcephalum*. As we move from the basal to distal region, the contact angle (θ) was found to vary in the range of 120–136° for both the species. Moreover, the wing of the dragonfly was seen to be more hydrophobic than that of the damselfly one. An attempt has also been made to link roughness factor (r_φ) and solid-water fraction (φ) through the simplified Wenzel and Cassie-Baxter models. We noticed that, r_φ and φ tend to follow a linear relation that gives $r_\varphi = 1.47$ in the limit, $\Delta\theta < 10.1°$, latter being recognized as the difference in angle between the measured CA over a surface to that of the CA (~105°) known for a smooth surface. Our experimental data, however, revealed empirical relations which predicted higher r_φ values, particularly when $\Delta\theta$ is large. While the overall reflectance response of the distal segment was believed to be stronger than that of the basal part, the edge parts of the dragonfly and damselfly wings exhibited exponential associated growing trends with increasing wavelength. The relative reflectance response, corresponding to ~494 nm and 370 nm peaks, gets nearly doubled for the edge specimen as compared to the distal and basal parts. The edge- specimen, which comprises of rectangular shaped, periodic microstructures, displayed carotenoid based two broad peak maxima at ~422 nm and ~494 nm. The surface roughness which arises through the distribution of oblate-shaped nano-fibrils is believed to be the basis of sub-surface volume scattering. Interrelating nanostructure surface roughness based wettability and reflectance characteristics would provide new insights on structure-property relationship in naturally available soft matter systems including templates of biological origin.

1. Introduction

Wetting of rough surfaces is a complex problem which continues to attract scientists, particularly due to the emergence of new, functional materials that might offer desired surface structure at micro as well as nanoscale level [1]. The wettability of solid surfaces is an important property, which is dictated both by the chemical composition and surface architecture of well defined geometry [2]. While wetting refers to spreading of liquid on a solid substrate, the nature of wetting-dewetting phenomenon is pertinent to numerous industrial applications [3]. During the past decade, surface roughness based superhydrophobicity and self-cleaning action, have emerged as an active field of research. Essentially, the hydrophobic surface has a water contact angle (CA) greater than 90°. In contrast, the superhydrophobic surface is characterized by a CA greater than 150°. In this regard, the densely packed aligned carbon nanotube (ACNT) surfaces are shown to exhibit CA values as large as 160°, both for oil and water drops [4]. Moreover, various superhydrophobic surfaces with inclusion of functional materials (e.g., ZnO, TiO_2, CNT, silica, silver etc.) are shown to be extremely effective as regards, self cleaning and anti-adhesion characteristics [5]. For instance, snow sticking, contamination, oxidation, current conduction etc. are greatly inhibited on such superhydrophobic surfaces [6]. These superhydrophobic surfaces have gained much interest owing to its usefulness in daily life as well as in industrially relevant measures [7]. In the past, many artificial surfaces with special wettability property have been processed through numerous methods, and to name a few are, template assisted [8], sol-gel processing [9], self-assembly [10,11], electrochemical [12], electrospinning [13], electro-less deposition [14], chemical etching [15] and chemical vapour deposition (CVD) methods [16] etc.

On the other hand, one can also observe wetting-dewetting features (including superhydrophobicity) in natural systems, such as, plants and insects. For instance, a lotus leaf offers an excellent

* Corresponding author.
E-mail addresses: best@tezu.ernet.in, dmohanta1973@gmail.com (D. Mohanta).

http://dx.doi.org/10.1016/j.apsusc.2016.06.049
0169-4332/

superhydrophobic surface where beads could be formed spontaneously, which then tend to roll off the leaf taking away all the dirts along the way (*Lotus effect*) [4,17]. Such an event arise due to two levels of rough structure at the immediate surface of the leaves that comprise of both micrometer-scale bumps as well as nanometer-scale hair like make-ups and the waxy composition of the surface. Besides plants, noticeable dewetting response can be witnessed in the avian systems, the insects, like water strider, beetle, moth, butterfly, damselfly etc. Not surprisingly, a large class of insects, moths and flies fly in the rain without getting wet owing to their structurally impermeable wings. The dewetting response of these insect wings is believed to alter with the surface construction and microscopic geometry there in, thus giving rise to a very high water CA. In particular, almost all dragonflies fly in the rain without getting wet [18]. Exploiting the non-wetting property of a dragonfly wing is of fundamental importance for directing research towards making suitable artificial surfaces. In the past, the wettability of a dragonfly's wing was largely referred to its cuticle wax surfaces [19,20]. The stenocara beetle found in the Namib desert could collect drinking water from the fog-laden wind on their backs. These droplets are formed by the insect's bumpy surface, which consists of alternate hydrophobic (wax-coated) and hydrophilic (non-waxy) regions [21]. The water strider's legs show good water repellent property due to its unique microstructure pattern for which CA is nearly 167° [22]. The butterfly wings too exhibit hydrophobic characteristics on which water drops can move freely along certain direction. The wettability of pigeon feather has also been worked out with the proposition that the Cassie-Baxter wetting regime is inherent in the pigeon pennae [23,24]. A two-fold hierarchical pattern comprising of barbs and barbules was believed to be mainly responsible for displaying larger CA values and water repellency.

While evaluating wetting-dewetting phenomena, the nature of surface roughness is typically assessed for all types of above mentioned species. The Wenzel model is employed to represent the collapsed state of the drop, whereas suspended state of the drop is dictated by the Cassie-Baxter approach [19,24]. It is not known however the limit of CA that predicts any departure from the condition of a smooth-flat surface while working with both the models, simultaneously. On the other hand, vizualizing surface roughness both by CA and reflectance/transmittance measurements is rarely discussed in the literature. In this work, considering wings of the dragonfly and damselfly as the test-bed, we exploit hydrophobic behavior of the specimens while moving from one region to the other across the wing surface. It is worth mentioning here that, both the specimen types belong to the order *Odanata*. The specimens are special in the sense that, dragonfly wings are kept fully extended and stay flat away from the body when at rest, while the damselfly wings are held back together across the body crossed. Unlike many other insects, a dragonfly is fully dependent on its wings for movement since it cannot walk with the help of legs. Usually, the time of flight of a dragonfly is comparatively larger than that of a damselfly species. The present work demonstrates an attempt to connect surface roughness with dewetting and reflectance responses after evaluating a simplified model on roughness factor and water solid fraction.

2. Experimental: materials and methods

2.1. Sample specimens

The specimens to be investigated are basically the hindwings of a matured female dragonfly of *Odanata* order acquired from natural environment during post-monsoon season (Fig. 1). The sample dragonfly (*Gynacantha Dravida*) was belonging to the family of *Aeshnidae* and order *Odanata* reported to be found in the western ghat, eastern and north-eastern regions of India. While the abdomen of the dragonfly measures 4.4 cm long, the respective length and breadths of the wings are found as, ~4.5 cm and 1.5 cm (Fig. 1(a)). The enlarged view of the hind wing is acquired through 10× microscopic imaging, shown in Fig. 1(b). It illustrates a great variety of polygons, both in size and shape as one moves along the length and across the breadth. The other specimen considered was a blue riverdamselfly (*Pseudagrion Microcephalum*) and belonging to the family *Coenagrionidae*, order *Odanata* and suborder *Zygoptera*. The digital and 10× microscopic photographs of the wing are depicted in Fig. 1(c) and (d); respectively. Although in some earlier works chemically treated wings are employed in order to minimize the time dependent changes of the surface properties [25], here the samples are left untreated to restore the chemical and physical properties of the cuticle and waxy layer. The portion of the wing close to the abdomen is recognized as the basal part, while the region away from the abdomen is termed as the distal part. The basal, central and distal parts of the dragonfly and damselfly hindwings are chosen for assessing dewetting/hydrophobic responses exploited through CA measurements.

2.2. Water contact angle (CA) measurements

A custom made contact angle setup is employed for CA studies in the static mode. First, the desired wing specimen is kept horizontally on the platform of an XYZ stage that has 3D movement. One droplet of water of volume ~80 μl is then gently placed over the region under study. An independent PC—interfaced microscopic camera (Digimicro, 10×), fixed on a vertical stand, was screw-adjusted to image the solid-water interface along with the whole water droplet itself. The CAs are measured several times over the basal, central and distal segments of the hindwing separately. The top view and the side view of each of these parts have been captured for analysis. The image analysis was carried out by using *ImageJ software*® [26].

2.3. Imaging through optical and electron microscopy

The complex architecture of the dragonfly and damselfly wings are initially viewed under an inverted optical microscope (Leica DM IL LED) by employing a 20X objective. In this microscope, transmitted light is considered for optical imaging. Further, scanning electron microscopy (SEM, JEOL, JSM 6390 LV) was employed for detailed microstructure analysis of the given specimen. Prior to loading for SEM imaging, the surface of the specimens was subjected to a few nm layers of Pt coating to avoid charging effect during imaging. The images are captured at 10kX and 20kX to reveal microstructural details along with the chitinous elements that make up the fibrils.

2.4. Measurement through UV–VIS-NIR reflectance spectroscopy

The reflectance responses of the basal, distal and edge- regions of the hindwing are studied independently by using a UV–VIS-NIR spectrophotometer (2450 Shimadzu Co.). Since the overall spectra of the basal and distal were quite similar, we preferred to include a third specimen (edge-part) of the dragonfly wing instead of the central part. Owing to smaller wingspan of the damselfly we deliberated only off-central edge part of the specimen. The reflectance maxima were identified by way of deconvolution employing multi-peak Gaussian curve fitting technique. For assessing surface roughness feature of both the *Odanata* species, the edge specimens are preferred and analyzed for each case.

All the experiments were carried out at room temperature (300 K) and without chemical processing.

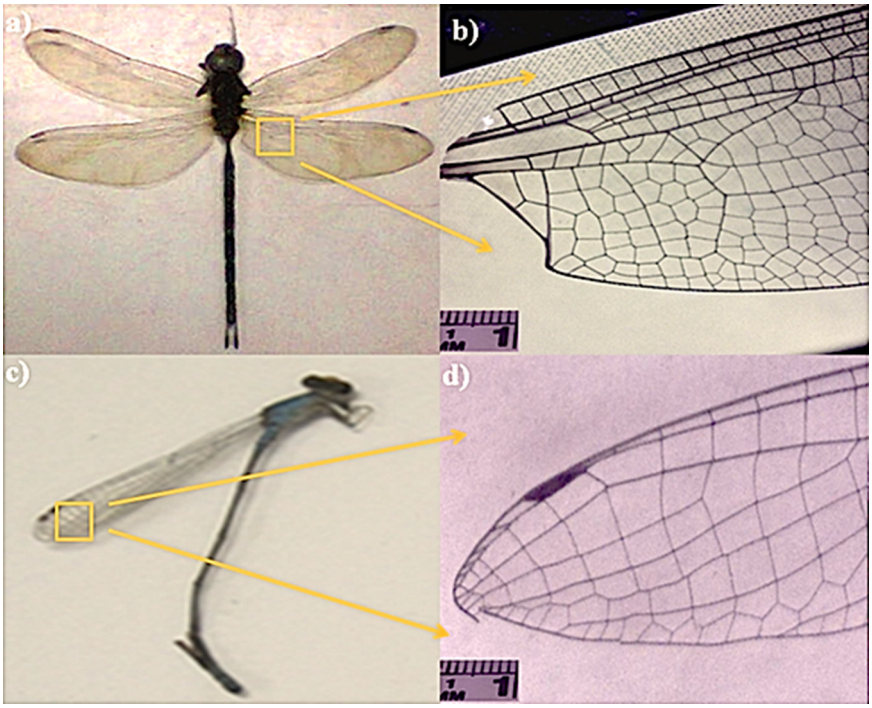

Fig. 1. (a) Digital photograph of the dragonfly (*Gynacantha Dravida*). An enlarged, microscopic view of the hind-wing is imaged by a 10× digicam, shown in (b). The digital and microscopic images of the hind-wing of the blue riverdamselfly are presented in (c) and (d); respectively. The scale bar shown in (b) and (d) represents 2 mm.

3. Results and discussion

The analysis with regard to electron microscopic imaging, dewetting feature and reflectance measurements are as detailed below.

3.1. Microstructural analysis of surface structure

Fig. 2(a)–(d) basically represent a set of micrographs of the dragonfly and damselfly wings examined under SEM. The microstructural network of both the wing types was found to comprise of a number of closed regions with cage-like morphologies. Essentially, the surface construction of the wing consists of polygonal makeups which appear in the form of rectangular, pentagonal and hexagonal units or combination of these. Each of the microstructure regions of the dragonfly wing is entrapped by five to six chitinous fibres that result in pentagonal and hexagonal structures (Fig. 2(a)). In contrast, square/rectangular-shaped morphology can be revealed as regards the hindwing of the blue riverdamselfly (Fig. 2(c)). This is, because, the dragonfly wing microstructure network has three-end junctions (shown by red arrows), whereas the damselfly wing structure contained four-end junctions (shown by blue arrows). The average span area of the polygonal unit is approximately, $\sim 10^5\ \mu m^2$. Each of the polygonal regions is bound by several hundred, micron size long (200–700 μm) chitin-based fibres, having an average thickness of ~21 μm and ~12 μm, as for the dragonfly and damselfly cases (Fig. 2(a),(c)). Occasionally, the side-fibres of the enclosed region contained short ridges that give thorn like appearances. The feature is more prominent in the dragonfly specimen, whereas damselfly specimen showed uniformly spaced bright spots on the side-edges, which may indicate broken positions of the thorns. The number of whole polygons was seen to increase as one moves from the basal to the distal region (Fig. 3(a)–(c)). Moreover, the triple junctions in all these three regions vary from one another. They are either Y-shaped or, T-shaped, but appear with varying dimensions. Some of them are perfectly T-shaped i.e., the angle between the fibre-stems is 90°, whereas the Y-shaped ones are characterized by at least one obtuse angle.

Essentially, the inside area of a polygon has a 2*d* membrane like planar architecture. At a higher magnification, we noticed the existence of randomly distributed oblate and rod- shaped units with tip-end diameters in the range of ~100–125 nm, as evident from the figure inset (Fig. 2(b),(d)). The damselfly specimen seems to have more extended regions unoccupied by chitin-oblates. The filled region of the damselfly specimen is however similar to the dragonfly species (Fig. 2(d)). At a higher magnification, the chitinous oblates were observed to be more tilted with occasional airgaps in the basal part (Fig. 3(d)–(f)). With pronounced packing characteristics, the packing density of the nanofibrils experienced by the distal part (~72/mm^2) is substantially higher than that of the basal section (~43/mm^2). The chitinous nanofibrils are spread in the central region with a moderate packing density of 50/mm^2. The overall spread of chitinous nano-oblates, to a great extent, gives an impression of the silt-filled black-tap road when viewed from a closer distance. It is important to note that, the mechanical strength and the flatness of typical wings are largely dependent on the nature of packing and microstructural polygonal design available in the wing part.

3.2. Water contact angle studies on hind-wing parts

In order to explore the hydrophobic response of different parts of the wing, we considered three prime regions, namely, basal (close to the insect-body), central and distal (farthest from the insect-body). The water CAs are measured in the vicinity of the indicated parts both for the dragonfly and damselfly wings repetitively. The side view of different parts can be found in Fig. 4 and measured angles are presented in Table 1. The wing surface, as one moves from the basal to the distal regions, gives a varying hydrophobic response and with a CA > 90°. The measured CA values are in the range of 120–136° and well below the superhydrophobic criterion (CA ≥ 150°) [22]. According to Wenzel, the homogenously developed cuticle wax surface is primarily respon-

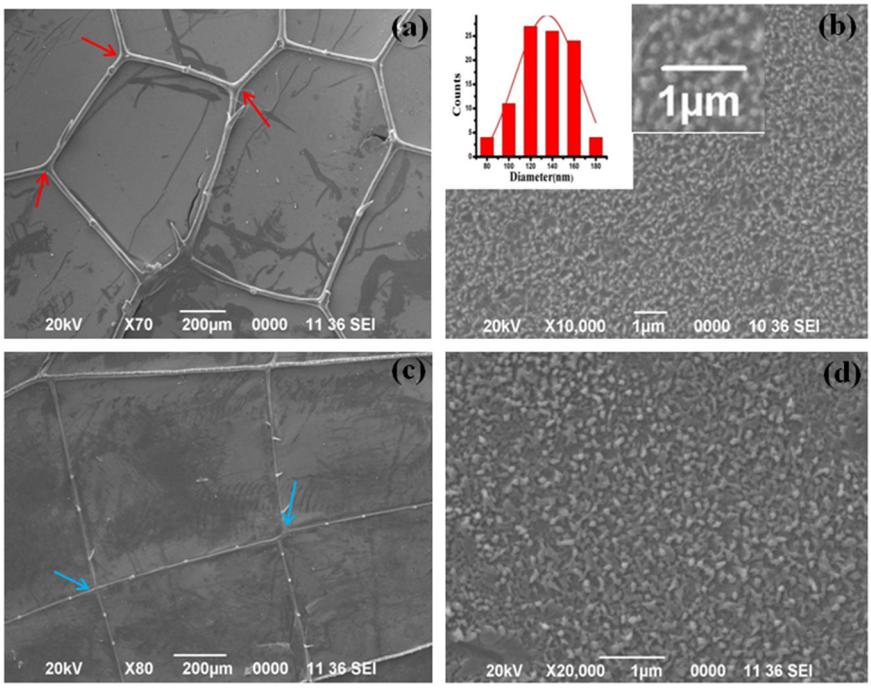

Fig. 2. SEM images of the central parts of (a,b) dragonfly wing and (c,d) damselfly wing. At a low magnification, microstructural polygonal network with triple (red arrow) and square (blue arrow) junctions are indicated in (a) and (c). The nano-oblate shaped randomly distributed fibrils present in the entrapped (polygonal) region are shown at (b) and (d). The inset is a histogram which depicts distribution of chitin-oblates with varying tip-end diameter. (For interpretation of the references to colour in this figure legend, the reader is referred to the web version of this article.)

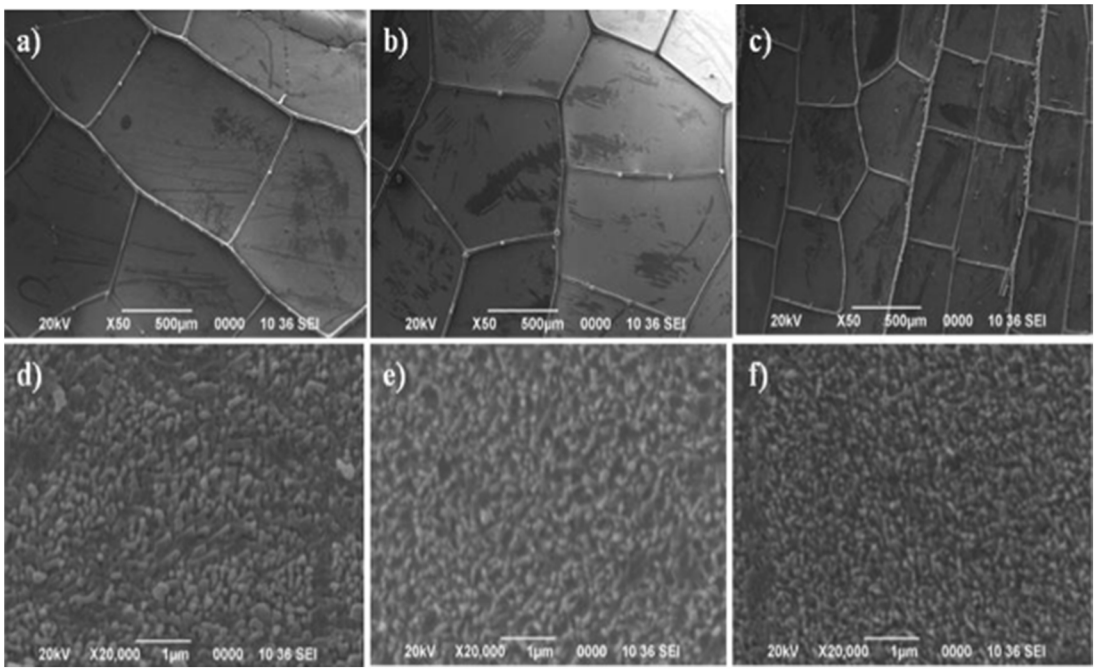

Fig. 3. SEM micrographs of (a) basal (b) central and (c) distal parts of the dragonfly hindwing captured at a lower magnification (upper panel). The magnified images are shown in sub-figures (d–f); respectively (lower panel).

Table 1
The water CA, surface roughness factor and water solid fraction measured through different experiments and models. The values corresponding to dragonfly and damselfly cases are separated by a comma in the same row.

Part of the wing	Average CA (degree)	Roughness factor, r_φ (Wenzel)	Water-solid fraction, φ (Cassie-Baxter)
Basal	121(±1), 123(±1)	1.98, 2.10	0.65, 0.61
Central	127(±1), 124(±1)	2.33, 2.16	0.53, 0.60
Distal	133(±1), 130(±1)	2.62, 2.48	0.43, 0.48

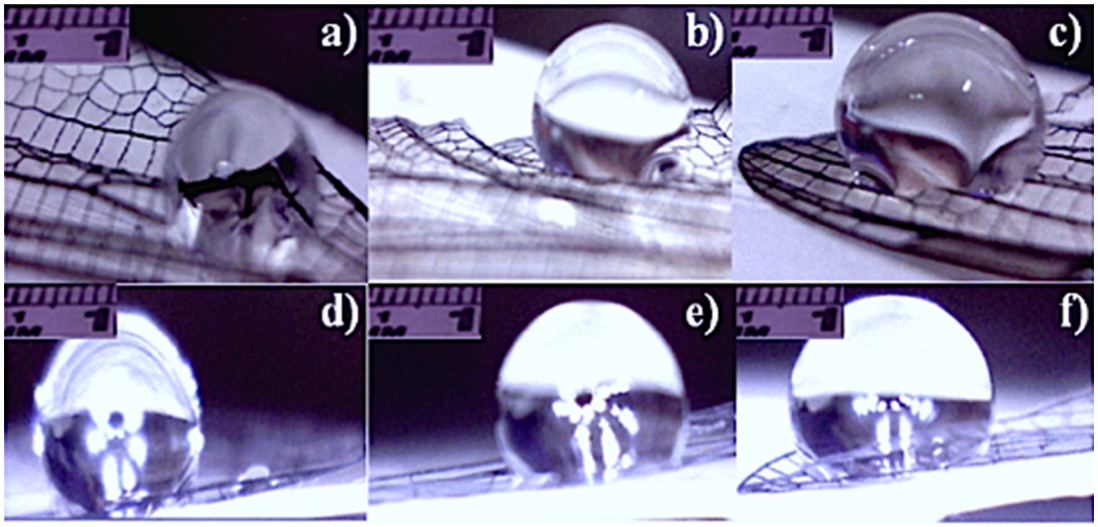

Fig. 4. The side view of the water droplets sitting on different parts of the hind-wing of the (a–c) dragonfly and (d–f) damselfly specimens. The basal, central and distal regions corresponded to (a,d), (b,e), and (c,f); respectively. The scale bar shown in each of the images corresponds to 2 mm.

sible for the hydrophobicity of the wing [27]. Although the nature of hydrophobicity is influenced by a number of factors, however chemical composition and surface morphology normally play dominant role. The distal part is observed to be more hydrophobic with respect to both the basal and central segments, in each species (Fig. 4(a)–(f), Table 1) [27]. It can also be noticed that, the base part of the water droplet shape is not perfectly flat, but forms curvy patterns with side-ends supported by the polygonal arms. For conducting CA experiments on flat surfaces, large sized drops are normally not considered in order to avoid the influence of the atmospheric pressure. Moreover, the size of the drop is kept smaller than the water capillary length (~2.5 mm) in order to avoid gravitational effect. Since an extremely small drop may get entrapped by the microstructure of bumpy rough surfaces, the CA measurements are dealt with drop sizes of comparable radii (~2.5 mm). A higher CA response of the distal part is due to the fact that, the region comprises of a sufficiently large number of microstructural polygonal units, as compared to the central and basal parts, and when all are covered with the water drops of similar size. Recently, it has been predicted that, a typical dragonfly wing would characterize a double surface roughness feature with fine and coarse segments [27]. Such a situation can arise when there is a tolerable variation in the surface roughness feature, which is quite different in the bound region (fine surface roughness) than that would be exhibited by the stiff fibrous stems (coarse roughness). Qualitatively, the surface roughness factor (r_φ) gives an idea about the overall roughness available in the specimen but gives no clue on how to isolate independent contributions accurately and precisely.

3.3. Assessment of theoretical models for wettability

The apparent water CA of a water drop on a typical rough surface can be explained either by using the Wenzel model or, the Cassie-Baxter model [28,29]. The Cassie-Baxter model generally describes the suspended state of a water droplet on a pillar-like rough surface, where it does not fill up the grooves and air is likely to get entrapped beneath the water drop. In contrast, the Wenzel model is applicable to surfaces where the droplet makes its way into the grooves, and therefore signifies the collapsed state. Typically, the size of the water drop is larger than the average dimension of the microstructural elements and thus can accommodate many units. When the droplet is large compared to the surface roughness, the droplet is withdrawn by the roughness and in that case, the Wenzel mode becomes more prominent [30]. According to Wenzel et al. [19,28], if θ and θ_w represent the respective water CAs of perfectly smooth and rough surfaces, then

$$\mathrm{Cos}\,\theta_w = r_\varphi \mathrm{Cos}\,\theta, \tag{1}$$

where, r_φ is the roughness factor and defined as the ratio between the actual surface area and the geometric projected area. Roughness factor, as the name suggests, gives the idea about the overall unevenness present at the specimen surface. For a smooth surface, $r_\varphi = 1$. The Cassie-Baxter approach is a modified version of the Wenzel model which accommodates the solid-water fraction, φ at the interface, and is given by:

$$\mathrm{Cos}\,\theta_c = \varphi(1 + \mathrm{Cos}\,\theta) - 1. \tag{2}$$

One can predict the limiting value of incremental CA by using the aforesaid equations independently and assuming $\theta = 105^\circ$ for a smooth surface proposed by Holdgate [20]. These two models are regularly used by the research community while examining hydrophobic surfaces and immiscible interfaces of technological interest. The coexistence of these models has also been predicted on the same surface [31]. Even though the Wenzel model is best suited to the collapsed state and the Cassie-Baxter model to the suspended state, provided that the increment, $\Delta\theta < \theta$, at equilibrium, one can write,

$$\theta_c = \theta_w = \theta + \Delta\theta,$$

and

$$\Delta\theta = (r_\varphi - 1)(\theta/2 - 1/\theta) \tag{3}$$

$$\Delta\theta = [(4 - \theta^2)(1 - \varphi)]/2\theta. \tag{4}$$

Here, Eqs. (3) and (4) are derived by expanding Cosθ in each of the Eqs. (1) and (2) and by neglecting higher order terms for the sake of convenience. For a very small increment in CA, i.e., for $\Delta\theta < \theta$, one can find a relation between r_φ and φ expressed by:

$$r_\varphi = [2 - \varphi(4 - \theta^2)]/(\theta^2 - 2), \tag{5}$$

and, thus we obtain

$$r_\varphi = -0.47\varphi + 1.47, \tag{6}$$

with $\theta = 105^\circ$, for a smooth surface and considering it in radian units. We noticed that, the above expression has a validity up to a maximum change of CA, $\Delta\theta_{\max} \sim 10.1^\circ$. The Eq. (6) essentially

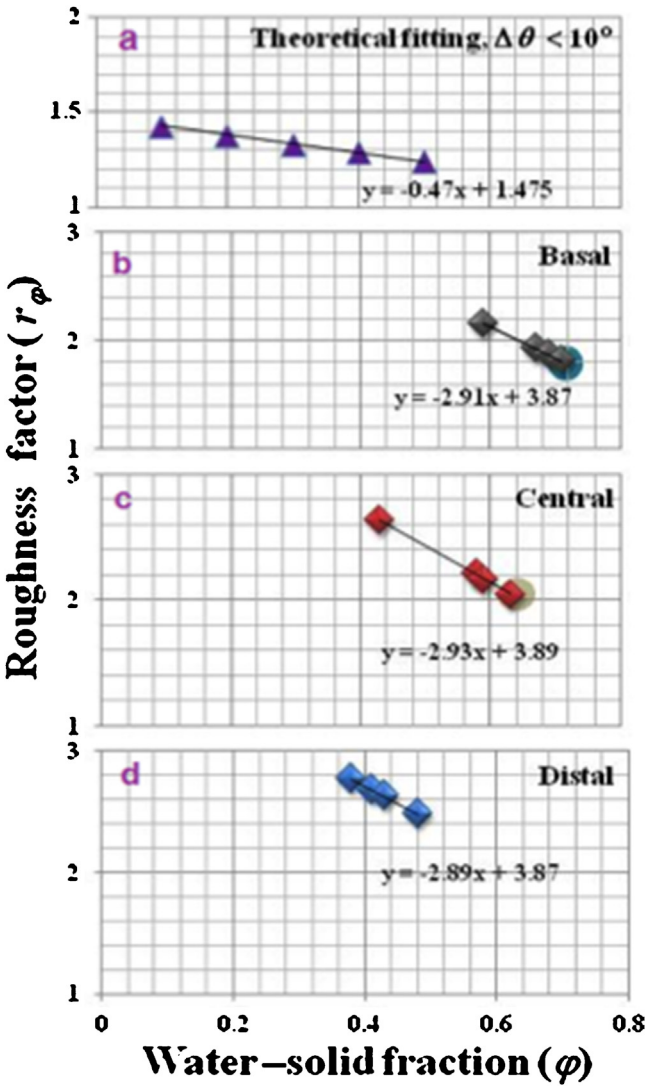

Fig. 5. The response of surface roughness factor vs. water-solid fraction in the (a) theoretical framework, and experimental results obtained from the (b) basal (c) central, and (d) distal parts of the dragonfly hind wing.

represents a straight line and with a negative slope, as can be found from Fig. 5(a). Apparently, with an increasing value of the water-solid fraction the surface roughness drops off slowly, giving $r_\varphi = 1.47$ when $\varphi = 0$, and $r_\varphi = 1$ when $\varphi = 1$ (smooth surface).

On the other hand, through repeated experiments performed on the basal, central and distal specimens, we found $\Delta\theta$ values as high as ~31° (Table 1). Using different data sets of measured CAs and employing Wenzel and Cassie-Baxter models to each part independently, r_φ and φ values are determined and their dependency for a given wing-type could be established. The individual characteristics corresponding to basal, central and distal segments of the dragonfly hindwing understudy are highlighted in lower three panels in Fig. 5(b)–(d). However, an average response for every part would give a common trend for the wing specimen. Accordingly, the dragonfly and damselfly wings were seen to obey the following empirical relationships:

$$r_\varphi{}^{dg} = -2.91\varphi + 3.88(\text{dragonfly}) \quad (7)$$

$$r_\varphi{}^{dm} = -2.81\varphi + 3.83(\text{damselfly})$$

Thus, the fly wings characterize similar trends with a slope variation close to 4%. We anticipate that, many flies belonging to *Odanata* order would follow this trend and provided that, $\Delta\theta$ is sufficiently large.

In a recent work, the wettability of *Odanata* species was shown to exhibit a strong dependency on the amount of epicuticular waxes [32]. In principle, roughness factor cannot be in isolation from the solid-water fraction though the former rely on geometrical construction, while the latter on the efficiency of adhesion. While mimicking natural surfaces of biological origin, their interrelation could help immensely in the construction of artificial hydrophobic surfaces with desired wettability. In this regard, not only dimension, but also ordering and shape of the inbuilt microstructural networks would play deterministic role on the behaviour of the surface structure. Accordingly, we have observed altered wetting response (CA) when moving from the basal region to the extreme end-part. Second, the distribution of oblate- shaped nanostructures also vary substantially as one moves from the basal to the distal region and more so that make-up the fibrous boundaries (Fig. 3). The empirical relations, as highlighted in Eq. (7) can be different for species of different order while belonging to the same class. This is because; the density of the nano-oblates within a bound region is capable of manifesting the wettability strength when a droplet of water comes in contact with the local surface structure. In case of the dragonfly wing under study, the reason behind exhibition of a higher CA and hydrophobic response of the distal region is chiefly due to the availability of large number of polygonal units and high packing density of nanoscale chitinous oblates entrapped within a unit.

3.4. Reflectance response of the hind wings and its linkage with surface roughness

Fig. 6(a) depicts a series of reflectance spectra corresponding to the basal, distal and edge parts of the dragonfly hindwing. The respective microstructural micrographs are shown on the right hand side of the spectra. The semi-transparent specimens gave multi- reflectance peaks in the visible region apart from a distinct peak located at ~275 nm due to the chitinous material present in the wing [33,34]. The peak at ~370 nm is relatively broad and asymmetric for both the basal and distal parts (Fig. 6(a)). Upon deconvolution through multi-peak Gaussian fitting on the basal and distal curves, we acquired two additional peaks located at ~422 nm and ~494 nm. It may be worth mentioning here that, the reflectance in the region 400–500 nm can be attributed to the presence of carotenoid, and therefore, the dip located at ~460 nm is ascribed to the absorption response of β–carotene [34]. The overall reflectance response, is stronger for the distal part than for the basal region. While moving from the basal to the distal region, the microstructural parameter tend to decrease (and nanostructure roughness increase) [27,35], as a result of which a higher r_φ, and water CA can be witnessed. We anticipate an improved reflectance response in the distal region owing to the availability of densely packed nano-oblate light scatterers beneath the cuticle. Nevertheless, any departure from the arrangement and periodicity of microstructural network introduces heterogeneity into the system and might suppress the reflectance response with increasing wavelength. Consequently, in the long wavelength regime, the reflectance is substantially repressed both for the basal and the distal parts. Earlier the nature of reflectance spectra has been extensively studied to unravel pigmentary and structural effects in butterflies [35–37]. Nanostructure surface mediated wettability as well as bifunctional characteristics, such as, anti-reflection property and super-hydrophobic response of *Cicada* wings have recently been demonstrated [38,39].

Unlike basal and distal parts, the edge- part of the dragonfly hind wing exhibited a much stronger reflectance feature, particularly in the long wavelength regime. Typically, the edge- part comprises

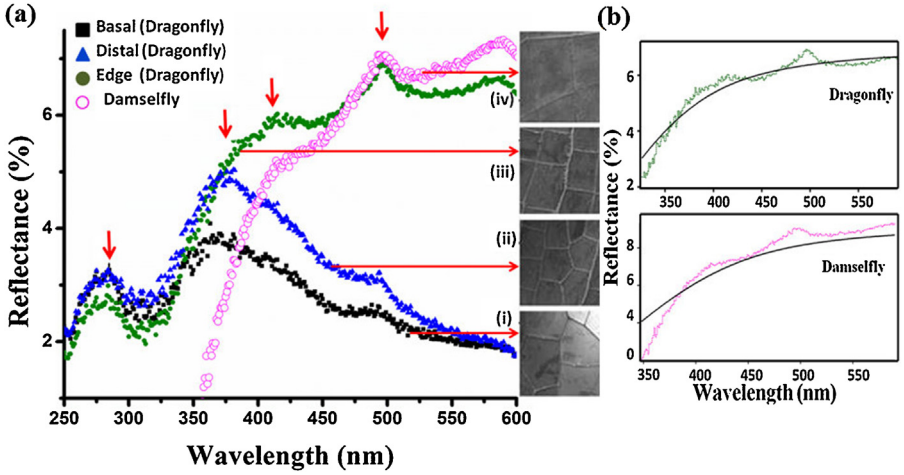

Fig. 6. (a) UV–vis reflectance spectra of the basal, edge and distal parts of the hind-wing of the dragonfly. As for the damselfly wing, response due to the edge-specimen only is presented. (b) The curve fitting features of the reflectance curves of the edge parts.

of highly ordered, rectangular (500 μm × 700 μm) microstructural units without any triple junction build up. It is worth mentioning here that, a high reflectance is realized when light scattered from the concerned interfaces appear in phase. This is possible when every surface layer present in the 2D chitinous plane has an optical thickness comparable to that of a quarter wavelength (λ/4). While realizing the average tip-end diameter of the randomly distributed chitin oblates and rods as approximately 125 nm (Fig. 2(b)), significant coherent scattering is expected to occur from these nano-structured elements, giving rise to a characteristic peak maximum at ~494 nm. An enhanced reflectance response may also be caused by multilayer interference occurring through thin chitinous elements and air-gaps. In this regard, existence of nearly 2–3 thin layers has been observed in the wings of a similar insect type, namely *Calopteryx Japonica* [40]. However, an overall growing reflectance trend with increasing wavelength, as noticed in the edge-specimen, calls for an analogy in terms of roughness limited scattering. The reason behind selecting this specimen is that, the edge-subpart would exist in every main-part of the wing, be it basal, central or distal. Moreover, the edge-part is free from the diverse microstructure types and is made up of only rectangular elements spread uniformly across the specimen.

Essentially, light scattering from a surface structure is characterized either by specular reflection or inelastic diffusive process. In order to assess reflectance response of a rough surface, we define root mean square roughness, r_μ, as the root mean square deviation of the surface-top from the mean surface level. Earlier, the specular reflectance at normal incidence for a polished conducting surface was put forward by Davies et al. as [41,42]:

$$R = R_0 \exp[-(4\pi r_\mu)^2/\lambda^2], \tag{8}$$

where R_0 is the reflectance of a perfectly smooth surface of the same material, λ is the incident light wavelength and that, λ and r_μ are measured in the unit of length. It may be noted that, r_μ has a characteristic dimension of length, but r_φ is a dimensionless entity (being a ratio of the actual surface area to the projected area). For a surface of biological origin, as in the present case, the overall surface feature accounts for two scattering processes: surface reflectance and sub-surface volume scattering. Since the edge-specimens of the dragonfly and damselfly wings are made of periodic arrangement of microstructural units along with the growing reflectance features with increasing wavelength (Fig. 6(b)), we intended to determine associated roughness parameters in these samples. The dragonfly wing gives a progressive reflectance curve, featuring a steep rise beyond 370 nm and exhibiting additional peak maxima at ~422 nm. The reflectance peak maxima, positioned at ~494 nm, are common features of both the dragonfly and the damselfly edge-specimens. As the specimen of the damselfly wing exhibited a rapid fall in the low wavelength regime, the edge-specimen, in this case might be a strong absorber of UV light (<350 nm). The relative strength of reflectance corresponding to ~494 nm and 370 nm peaks, both for the basal and distal segments of the dragonfly wing, is close to 0.7, which shoots up to ~1.4 in the edge-specimen (Fig. 6(a)). In other words, the association of periodic rectangular structures and inner surface irregularities present in the edge-part are chiefly responsible for growing reflectance characteristics at longer wavelength. In particular, plentiful nano-bumps would experience significantly high sub-surface volume scattering and hence, contribute more to the reflectance response in the extended visible region. By employing a standard software, the reflectance data sets of the edge parts were subjected to appropriate curve fitting over a broad wavelength range while ensuring a minimal chi-square value (Fig. 6(b)). The overall spectral response is close to the associated exponential curve fitting trend of the form given by:

$$R = R_0[1 - \exp(-\lambda^2/r_{\mu v}{}^2) - \exp(-\lambda^4/r_{\mu s}{}^4)]. \tag{9}$$

This is quite different from the representative feature of the polished conducting surfaces given in Eq. (8). Here, $r_{\mu s}$ and $r_{\mu v}$ characterize average surface roughness contributions associated with the surface reflectance and the sub-surface volume scattering; respectively. Consequently, as for the dragonfly edge specimen, the respective roughness parameters are estimated to be $r_{\mu s} \sim 368.5$ nm and $r_{\mu v} \sim 241$ nm. The respective parameters for the damselfly wing are, ~372 nm and 280 nm. The submicron roughness, $r_{\mu s}$ is comparable to ~370 nm peak maxima and is believed to have originated from the overall surface make up of chitinous nano-oblate assemblies undergoing specular reflection. In contrast, $r_{\mu v}$ is a consequence of diffusive scattering aroused via curved surfaces and interfaces between chitin oblates. We anticipate that, it is $r_{\mu v}$ which really matters for water repellency and thus can be linked to r_φ.

In order to deal r_φ and $r_{\mu v}$ on equal footing, the latter needs to be standardized with the two strong peak maxima which characterize carotenoid support, i.e., $\lambda_m = 422$ nm and 494 nm. These are the characteristic wavelengths meant for coherent scattering events. In this situation, roughness factor can be redefined as, $r_{\mu v}{}' = \lambda_m/r_{\mu v}$. Consequently, the dragonfly specimen can have $r_{\mu v}{}'$ in the range of 1.75 and 2.05. The damselfly specimen has $r_{\mu v}{}'$ between 1.5 and 1.76. When these values are fitted for r_φ in the empirical Eq. (7), we noticed that, the effective water-solid fraction, φ takes a value

between 0.62 and 0.73. This is indicated by shadowed circles at the tail-end of the basal and central-parts of the dragonfly hind-wing (Fig. 5). In the absence of repetitive measurements of CA and reflectance response from various parts of the damselfly wing, such a connection could not be made with certainty. This is because, the wing span was not only thin but also mechanically unstable. It was extremely difficult to extract complete diffusive scattering occurring within a confined geometry, because localized heating is likely to destroy the internal microstructure makeup. In this backdrop, a direct connection between the overall reflectance feature and wetting property may be realistic with advanced versions of reflectance spectroscopies including polarization dependency and total internal reflection aspects into account. Nevertheless, apart from composition, studies as regards isolation of nanostructure surface roughness that govern dewetting response and superhydrophobicity in certain biological specimens are in progress.

4. Conclusions

The hydrophobic and reflectance responses of two *Odanata* species have been demonstrated through CA measurements and reflectance spectroscopy; respectively. A simplified model is worked out assuming Wenzel and Cassie-Baxter models to hold simultaneously. In both the dragonfly and damselfly wings, the distal parts are found to be more hydrophobic than the other parts owing to the exhibition of a relatively higher CA in the former case. We anticipate an improved surface structure in this part owing to the availability of relatively densely packed chitinous nanofibrils. Appropriate empirical relations connecting r_φ and φ have been worked out for the parts independently, as well as collectively with an average effect. The overall reflectance is observed to be stronger in the distal part than the basal counterpart. In contrast, the edge-parts showed a growing reflectance trend along with the exhibition of broadened peak maxima at ~422 nm and 494 nm, for both the dragonfly and damselfly wings. The analysis of reflectance spectra of the edge specimens provided a clue to interrelate sub-micron surface roughness with the roughness factor, and consequently with the hydrophobic response. The scope of interrelating optical window and microstructure roughness can be widened further to unravel bifunctional features in a more precise manner, which is underway.

Acknowledgments

The authors thank Mr. R. Boruah for extending help in SEM imaging. We also acknowledge peers and colleagues for their valuable suggestions.

References

[1] M. Nosonovsky, B. Bhusan, Green Tribology, Green Energy and Technology, Springer-Verlag, Heidelberg, 2012.
[2] R. Blossey, Nat. Mater. 2 (2003) 301.
[3] D. Quere, P.-G. de Gennes, F. Brochard-Wyart, Capillarity and Wetting Phenomena: Drops, Bubbles, Pearls, Waves, Springer Science and Business Media, 2004, pp. 13.
[4] J. Genzer, K. Efimenko, Recent developments in superhydrophobic surface and their relevance to marine fouling: a review, Biofouling 22 (339) (2006).
[5] H. Teisala, M. Tuominen, M. Aromaa, M. Stepien, J.M. Makela, J.J. Saarinen, M. Toivakka, J. Kuusipalo, Langmuir 28 (2012) 3138.
[6] S. Dai, D. Zhang, Q. Shi, X. Han, S. Wang, Z. Du, CrystEngComm 27 (2013) 5389.
[7] Y.Y. Liu, R.H. Wang, H.F. Lu, L. Li, Y.Y. Kong, K.H. Qi, J.H. Xin, J. Mater. Chem. 17 (2007) 1071.
[8] H.S. Hwang, S.B. Lee, I. Park, Mater. Lett. 64 (2010) 2159.
[9] S.S. Latthe, H. Imai, V. Ganesan, A.V. Rao, Appl. Surf. Sci. 256 (2009) 217.
[10] M. Kemell, E. Färm, M. Leskelä, et al., Phys. Status Solidi A 203 (2006) 1453.
[11] J. Ji, J.H. Fu, J.C. Shen, Adv. Mater. 18 (2006) 1441.
[12] M. Li, J. Zhai, H. Liu, et al., J. Phys. Chem. B 107 (2003) 9954.
[13] Y. Zhu, J. Zhang, Y. Zheng, et al., Adv. Funct. Mater. 16 (2006) 568.
[14] X.H. Xu, Z.Z. Zhang, J. Yang, Langmuir 26 (2010) 3654.
[15] B.T. Qian, Z.Q. Shen, Langmuir 21 (2005) 9007.
[16] A. Cremona, E. Vassallo, A. Merlo, et al., J. Mater. Res. 23 (2008) 1042.
[17] C. Neinhuis, W. Barthlott, Ann. Bot. 79 (1997) 667.
[18] F. Song, K.W. Xiao, K. Bai, Y.L. Bai, Mater. Sci. Eng. A475 (2007) 254.
[19] R.N. Wenzel, Ind. Eng. Chem. 28 (1936) 988.
[20] M.W. Holdgate, J. Exp. Biol. 32 (1955) 591.
[21] A.R. Parker, C.R. Lawrence, Nature 414 (2001) 33.
[22] X.-Q. Feng, X. Gao, Z. Wu, L. Jiang, Q.-S. Zheng, Langmuir 23 (2007) 4892.
[23] E. Bormashenko, Y. Bormashenko, T. Stein, G. Whyman, E. Bormashenko, J. Colloids Interface Sci. 311 (2007) 212.
[24] A.B.D. Cassie, Discuss. Faraday Soc. 3 (1948) 11.
[25] C.W. Smith, R. Herbert, R.J. Wootton, K.E. Evans, J. Exp. Biol. 203 (2000) 2933.
[26] http://imagej.nih.gov/ij/.
[27] C.-Y. Gao, G.-X. Meng, X. Li, M. Wu, Y. Liu, X.-Y. Li, Xin Zhao, I. Lee, X. Feng, Surf. Interf. Anal. 45 (2013) 650.
[28] R.N. Wenzel, J. Phys. Colloids Chem. 53 (1949) 1466.
[29] A.B.D. Cassie, Contact angles, Discuss. Faraday Soc. 3 (1948) 11.
[30] Akira Nakajima, NPG Asia Mater. 3 (2011) 49.
[31] A. Giacomello, S. Meloni, M. Chinappi, C.M. Casciola, Langmuir 28 (2012) 10764.
[32] S.H. Nguyen, H.K. Webb, J. Hasan, M.J. Tobin, D.E. Mainwaring, P.J. Mahon, R. Marchant, R.J. Crawford, E.P. Ivanova, Vib. Spectrosc. 75 (2014) 173.
[33] R. Stoddart, P.J. Cadusch, T.M. Boyce, R.M. Erasmus, J.D. Comins, Nanotechnology 17 (2006) 680.
[34] R. Boruah, P. Nath, D. Mohanta, G.A. Ahmed, A. Choudhury, Nanosci. Nanotechnol. Lett. 3 (2011) 458.
[35] B.D. Wilts, P. Pirih, D.G. Stavenga, J Comp. Physiol. A Neuroethol Sens Neural Behav Physiol. 197 (2011) 693.
[36] S. Kinoshita, Structural Colors in the Realm of Nature, World Scientific Publishing, Singapore, 2008, pp. 112.
[37] Y. Ding, S. Xu, Z.L. Wang, J. Appl. Phys. 106 (2009) 074702.
[38] L. Dellieu, M. Sarrazin, P. Simonis, O. Deparis, J.P. Vigneron, J. Appl. Phys. 116 (2014) 024701.
[39] M. Sun, G.S. Watson, Y. Zheng, J.A. Watson, A. Liang, J. Exp. Biol. 212 (2009) 3148–3155.
[40] T. Hariyama, M. Hironaka, H. Horiguchi, D.G. Stavenga, in: S. Kinosita, S. Yoshioka (Eds.), Structural Colors in Biological Systems, Osaka Univ Press, Osaka, 2005, p. 153.
[41] H. Davies, Proc. Inst. Electr. Eng. 101 (1954) 209.
[42] H.E. Bennett, J.O. Porteus, J. Opt. Soc. Am. 51 (2) (1961) 123.

J Bionic Eng 15 (2018) 1012–1024
DOI: https://doi.org/10.1007/s42235-018-0089-6

Journal of Bionic Engineering
http://www.springer.com/journal/42235

Surface-wettability and Structural Colouration Property of Certain *Rosaceae* Cultivars with Off-to-dark Pink Appearances

Swati N Aideo, Dambarudhar Mohanta*

Nanoscience and Soft Matter Laboratory, *Department of Physics*, *Tezpur University*, *Napaam*, *Tezpur*-784028, *Assam*, *India*

Abstract

The present work reports microstructure-based wettability and reflectance responses of three varieties of Indian *Rosaceae* (*Rosa*) cultivars, *viz*. white rose (*Rosa chinensis var spontanea*), light pink rose (*Rosa chinensis var minima*) and dark pink rose (*Rosa chinensis var minima*). As for wettability, static and advancing and receding Contact Angles (CA) have been measured, for each type of matured rose petals. The surface roughness factors (r_φ), which are largely dependent on the micro-papillae assembly within the rose petal, are estimated to be, 2.74, 2.27 and 2.94 in case of White (W), Light Pink (LP) and Dark Pink (DP) petals; respectively. Moreover, the respective Contact Angle Hysteresis (CAH) values are measured as 51˚, 27˚ and 59˚. In order to exploit structural colouration through the reflectance characteristics, the specimens were dipped in three different media of different Refractive Indices (*RI*), *viz*. ethanol (*RI* = 1.36), propanol (*RI* = 1.39) and glycerine (*RI* = 1.47) for about 24 h. Upon ethanol and propanol adsorption, the LP and DP rose petals showed unusually similar reflectance patterns over a wide range of wavelengths, thus indicating a common microstructural share and structural colour contribution. The wetting-dewetting and structural colouration in natural systems, to a great extent, are dictated by the surface structure and solid-liquid and liquid-air interfaces, not only offer fundamental interest but also give scope for mimicking in artificial designs of technological interest.

Keywords: microstructure, surface roughness, wettability, structural colour, reflectance

1 Introduction

Nature provides innumerable examples of living systems which are known to display two important, yet distinctly different phenomena: structural colouration and wettability property. Natural systems are coloured due either to pigmentary constituents present within the system, or due to its microstructural build-up that results in structural colour[1]. In plant kingdom, among flowers, *Rosaceae* (rose family) finds a distinct place not only by virtue of its brilliant appearance but also due to its placid fragrance, while captivating the attention of many bystanders. In the recent past, the bright colours and diverse varieties of rose have stimulated research interest to exploit underlying phenomena in these delicate specimens. With a biochemical perspective, the pigmentary or chemical colours have been extensively studied in naturally occurring species and it was found that, the colours due to these macromolecular constituents are generally dull, owing to the absorption of only certain wavelengths of light[1,2]. In contrast, the structural colour arises as a result of highly select microstructural make-ups, which largely dictate the surface feature of the specimen under consideration. In other words, patterned surfaces and sub-surfaces normally participate in structural colouration by way of numerous light scattering events at appropriate angles. There exist, numerous naturally occurring photonic structures which display tuneable structural colour[3]. The examples include, but not limited to butterflies, bird feathers, beetles, insects and flower-bearing plants[4–10]. Recently, the hyperfine ultrastructure of *Trogonoptera Brookiana* studied by Han *et al.* gave indication that these structures are sensitive to liquid medium[11]. While viewing under 3D microscope, they also witnessed the discolouration effect of the scales in response to the liquid medium. The bright, iridescent colour normally occurs in the nanoscale architecture of confined geometry, which is capable of producing a narrow-band spectral purity but of ultrahigh reflectivity[1].

The colour characteristics have been studied in great detail particularly, in insect covers, aquatic species

***Corresponding author:** Dambarudhar Mohanta
E-mail: best@tezu.ernet.in

and in bird feathers; but scarcely in plants because of its rapid change of microstructure with aging and also due to physiological reasons. A report on flowers, primarily *Hibiscus Trionum* suggests iridescence as a unique property of structural colour which mainly depends on the microscopic diffraction gratings present in the flower petal[12]. In plants, along with the diffraction grating feature, the regularly spaced ridges and spacing are capable of enabling multiple interference, which in turn offer bright colour to the flowers[13]. Moreover, the optical features of the petals were shown to be strongly dependent on the types of cell forming tissues and with the surface covering in the form of nanoscale gaps and patterning[14]. The intrinsic assembly of the diffraction gratings of the flower petal is believed to be used by the bees and select flies as cues for precise identification of the naturally rewarding flowers[2].

On the other hand, the wetting-dewetting property of natural specimens is a vital aspect which helps in predicting the physiological state and environmental stability at large. The lotus (*Nelumbo Nucifera*) and taro (*Colocacia Esculenta*) leaves are excellent examples of non-sticky, super-hydrophobic surfaces that allow water droplets to roll off easily (water Contact Angle, CA $>150^{\circ}$)[14]. The super-hydrophobic surfaces exhibit excellent water repellency and are obvious choices for self-cleaning action. As regards wettability property and structural colour, independent studies have been made previously on different rose varieties along with the characteristic rose petal effect[1,14,15]. However, a qualitative account connecting wettability and structural colouration of these soft, delicate specimens has not yet been addressed. Furthermore, the colour-spread in the chromaticity diagram before and after chemical processing is rarely discussed in the literature. The present work highlights a comparative view on microstructural make-ups, reflectance and wettability features of certain rose cultivars belonging to *Indian Rosaceae* family and with off-to-dark pink appearance.

2 Materials and methods

2.1 Specimen collection

The specimens opted for our work were three varieties of the *Rosaceae* cultivars, namely, white rose (*Rosa chinensis var spontanea*), light pink rose (*Rosa chinensis var minima*), and dark pink rose (*Rosa chinensis var minima*) and labelled as, W, LP and DP; respectively. To retain surface property, specimens were generally collected prior exposure to direct sun light. Accordingly, fresh flower specimens were gently collected from our university garden during morning hours. Moreover, in order to retain the physiological state intact, the time gap between the plucking of flower and actual experiment was kept minimum (< 60 min), for every sample. The average dimension of the petals examined varied in the range of 12 mm – 25 mm. In order to exploit the nature of discolouration effect each of the specimens was treated with ethanol, propanol and glycerine separately (Fig. 1).

2.2 Microstructural assessment of rose petals

Apart from capturing images with the help of a digital camera, morphological details of the specimens could be revealed by employing a scanning electron microscope (JEOL, JSM-6390LV), working at 20 kV. The sectioned specimens were subjected to several nanometer platinum coatings in order to prevent the surfaces from charging effect during imaging. In order to extract detailed information about a particular region, micrographs were captured at different magnifications.

2.3 Wettability study on rose petal surface

The wetting-dewetting features of the specimens were carried out through measuring static water Contact Angles (CA) by employing a contact angle meter (Kyowa Interface Science Co.Ltd.). At first, ~3 μL volume droplet of water is gently placed on the petal specimen mounted on the base plate positioned in between the locations of a white light source and CCD camera meant for imaging. The tilting base methodology was also employed to measure the advancing and receding angles and consequently, the Contact Angle Hysteresis (CAH). This forms an important part in understanding the wetting-dewetting feature of a system under study. The base of the petal surface was subjected to an intermittent tilt mode, and the tilt was varied in the range of 0° – 90°. Advancing (maximum) and receding (minimum) angles were measured with a repetition of 10 times for every degree of tilting. The data acquisition was made on a PC equipped

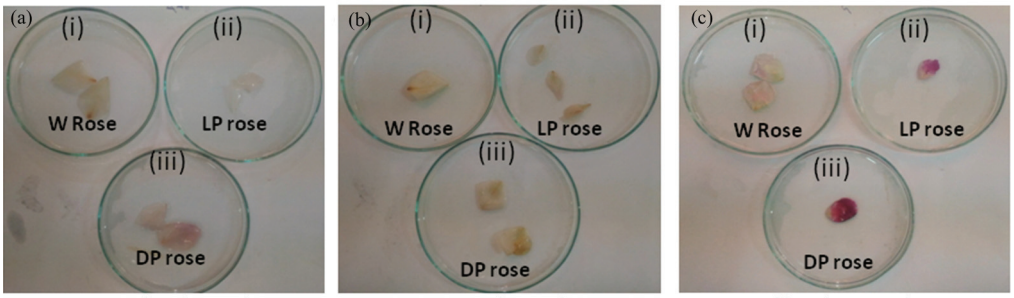

Fig. 1 Treatment of rose petals with immersion in (a) ethanol, (b) propanol and (c) glycerine. The labels (i), (ii) and (iii) essentially represent white (W), light pink (LP) and dark pink (DP) rose petals; respectively.

with the standard FAMAS software®.

2.4 Spectral response and chromaticity diagram

In order to exploit optical features of the flower petals, UV-Vis-NIR reflectance spectroscopy (Shimadzu Co.) has been employed in ambient environment. Moreover, in order to evaluate the structural and pigmentary contributions qualitatively, the whole rose-petals were treated with different organic media of known Refractive Indices (*RI*) *viz.* ethanol (*RI* = 1.36), propanol (*RI* = 1.39) and glycerine (*RI* = 1.47). Accordingly, the reflectance spectra of the untreated and treated specimens were acquired and analysed. The air gaps and voids to be temporarily filled by these liquids were believed to affect the spectral behaviour immensely over a given range of wavelengths. Moreover, using the reflectance data of the rose petals, appropriate CIE chromaticity diagrams were plotted using CIE 1931 colour space[16].

All the experiments were carried out at room temperature. The experimental results were discussed in the light of some theoretical treatment while discussing structural colouration and wettability feature of different cultivars, on a comparative basis.

3 Results and discussion

The wettability and structural colour characteristics of the *Rosaceae* family were analysed for each specimen type under ambient conditions. Similar experimental conditions were also set by Kinoshita while studying structural colour in *morpho* butterflies[17].

3.1 Microstructural analysis of rose petals

The digital snap-shots as well as SEM micrographs (captured at different magnifications) of the White (W), Light Pink (LP) and Dark Pink (DP) roses are depicted in Fig. 2. While the appearance of flowers clearly illustrates varied colour strength, the micrographs showed numerous micro-papillae assemblies with varying dimension, orientation and folds. The presence of micro-papillae, essentially the papillae on the rose petals appear with circular wrinkles or folds that are mainly responsible for enhancing the surface roughness of the petals[18]. Each of the papillae, essentially comprised of single cells, and therefore, every petal would contain several thousands of these micro-papillae. Further, the magnified SEM images depict the presence of nano-folders and nano-binders within each papillae. Even though each of the micro-papillae varies in dimension, distribution and orientation they exist in isolation from each other. Microscopically, the white rose petals signify aperiodic distribution of oblate to conical units at large (Fig. 2a). The light-pink petals, however, gave better homogeneity in terms of microscopic distribution of oblate units while they differ in dimension and tilt (Fig. 2b). As a result, the LP rose petals can have relatively more unfilled space within its surface structure. In contrast, the DP rose petal possessed round shaped micro-papillae, which gives the impression of a cage-like network (Fig. 2c). Nevertheless, the W and LP rose specimens offered short, elongated micro-papillae that are packed loosely or tightly at the regular surface sites. However, the periodic array of nanoscale entities within micro-papillae systems resembles photonic crystal structure, and might contribute considerably to the iridescence feature. The DP specimen, owing to its spectacular, periodic morphological micro-papillae assembly prohibits surface scattering events, to a great extent,

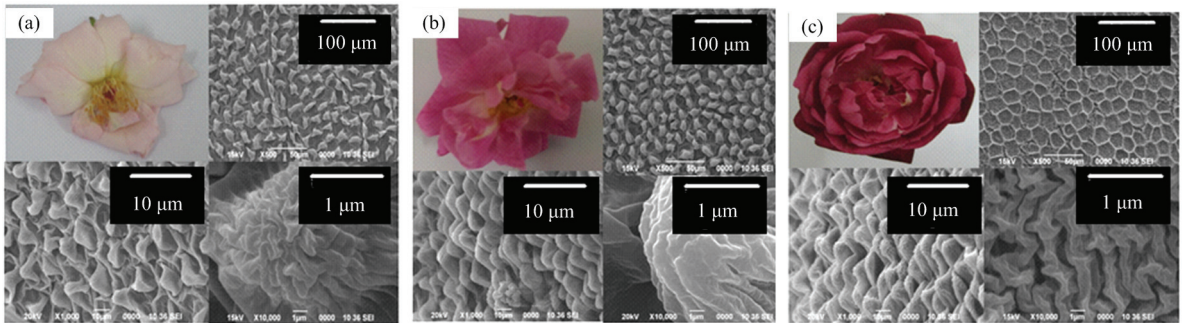

Fig. 2 SEM images of the three varieties of *Rosaceae* cultivars: (a) white (W), (b) light pink (LP) and (c) dark pink (DP) rose petals. The upper left corners depict digital snapshots of the rose specimens, whereas upper right corners highlight microscopic distribution of micro-papillae assembly, in each case. The lower panels illustrate SEM micrographs captured at higher magnifications. Note the dimension and orientation of the micro-papillae along with nano-folders within a single micro-papillae.

giving off deep, dark pink colour. This kind of micro-morphological periodicity can also be apprehended in butterflies, beetles, insect *etc*. which were believed to be the primary sources of iridescent structural colour[19]. A side view of the nano-folders and nano-oblates can be clearly seen at a higher magnification, for each rose-petal type. The physical parameters as regards, micro-papillae size, distribution *etc*. were determined directly from the micrographs and by employing Image J software®[20], as can be found in Table 1.

3.2 Surface wettability property of rose petals

3.2.1 Theoretical treatment and model on micro-papillae assembly

Two well accepted models are generally employed to describe wetting-dewetting phenomena: Cassie-Baxter (C-B) and Wenzel models[21,22]. The C-B model describes the suspended state of the liquid droplet, whereas, the Wenzel model explains the state of the droplet when the water fills up the grooves.

The contact angle of water droplet on any rough surface in the Wenzel mode is represented by:

$$\cos\theta_w = r_\varphi \cos\theta_f, \quad (1)$$

where r_φ is the roughness factor and θ_f is the contact angle on a flat, smooth surface.

Typically, contact angle in the C-B model is formulated as:

$$\cos\theta_c = \varphi(1+\cos\theta_f) - 1. \quad (2)$$

Here, φ represents the solid-liquid fraction.

It is worth mentioning here that, surface roughness and chemical composition both play dominant roles for displaying hydrophobicity[23]. On the other hand, the CA Hysteresis (CAH) is an important feature for examining (high or low) surface adhesion to water, especially for the hydrophobic surfaces[24]. Thus the determination of CAH is an important aspect while assessing hydrophobic/hydrophilic nature of the surface structure. In this regard, tilted plate methodology has been a versatile and proven technique for exploiting the advancing (max.) and receding (min.) angles of water droplet on a given sample under study and measured for different tilting angles[25]. As regards, CAH, two modes are already in place: rose effect and lotus effect. Generally, low hysteresis value indicates low solid-liquid adhesion, whereas, high CA hysteresis signifies a high solid-liquid adhesion[26]. A surface that has high CA as well as high CAH is said to exhibit rose petal effect, while, the lotus effect is displayed by a surface that has high CA and low CAH[14]. To be precise, surface roughness mediated adhesion could largely affect CAH and that, the pinning effect causes the droplet to stick to the surface. In this regard, being a unique surface phenomenon, the petal effect is characterized by a large CA, CAH and strong adhesion to water. Not surprisingly, a transition between the wetting regimes has also been predicted in earlier works[27,28]. Accordingly, different rose varieties can have petals with both high and low surface adhesion characteristics that largely depend on their surface microstructure[14]. In reality, for a surface make-up with sub-micron or nanoscale protuberances in each of the micro-papillae, water is believed to get adsorbed into the pockets of the air gaps slowly while

Table 1 Physical parameters of the *Rosacea* specimens under study

Specimen	Approximate base-width of the micro-papillae, d (μm)	Height of the micro-papillae, h (μm)	Aspect ratio, A_r	Micro-papillae peak-to-peak distance (pitch, p) (μm)	p/h
White rose (W)	11.06 ± 4.6	12.80 ± 6.5	1.16	15.95 ± 6.1	1.25
Light pink rose (LP)	9.78 ± 3.6	9.57 ± 4.5	0.97	15.20 ± 4.1	1.58
Dark pink rose (DP)	12.0 ± 4.5	12.65 ± 4.8	1.04	15.67 ± 4.6	1.23

undergoing a continuous transition from de-wetting to wetting point[28].

Referring to schematic illustrations, shown in Figs. 3a and 3b, physical parameters that would help in determining wetting and dewetting characteristics are: pitch value (p), diameter (d) and pitch-base height (h). The pitch value is defined as the average peak-to-peak distance between any two micro-papillae, whereas, pitch-base height represents the approximate height of the micro-papillae[28]. A smaller value of p/h ratio applies to the C-B regime, which tends to increase the static water CA. This ratio is important in the sense that, a lower value enhances the formation of air-pockets between the microstructures, and consequently, the water droplet cannot come in contact with the bottom surface[28]. In other words, when the effective contact area between the water droplet and the microstructure is minimized, the static CA increases for surfaces with low adhesion. Undoubtedly, numerous factors are quite responsible as far as hydrophobic feature of a surface make-up is concerned. For instance, for a water droplet of size comparable to the pitch value, bottom liquid may penetrate deep inside the grooves, but if the droplet is large enough then it will be supported only by the top surfaces of the pillars of the micro-papillae, forming numerous air gaps beneath the droplet base[29]. Not surprisingly, a surface with prevailing micro- and nanoscale roughnesses, the hydrophobic response is a consequence of the combined effect, though it is difficult to isolate individual contributions in a quantitative way.

For simplicity, the approximate microstructure roughness factor (r_φ) can be calculated by visualizing the micro-papillae as regular cylinders characterized by diameter (d), height (h) and pitch value (p) that can be found over a square area (Fig. 3b). The roughness factor, r_φ can be defined as the ratio of the actual, effective surface area to the projected, geometrical surface area. In a square area of length equal to the pitch value, the projected surface area is, p^2; whereas actual area is the sum of the curved surface area of the cylinder and the exposed surface area. To a good approximation, the actual surface area can be written as, $p^2+\pi dh$. Therefore, for a cylindrical system with its top being in contact with the water droplet[27],

$$r_\varphi = 1 + \frac{\pi dh}{p^2}. \tag{3}$$

The fraction of the solid-liquid contact under the droplet that would participate in the wetting-dewetting transition can be expressed as:

$$\varphi = \frac{\pi d^2}{4p^2}. \tag{4}$$

Combining the above two relations, one can interrelate surface roughness with the fractional solid-liquid contribution given as:

$$\varphi = \frac{d}{4h}(r_\varphi - 1). \tag{5}$$

The aforesaid parameters for the rose petals under study are enlisted in Table 1 and Table 2.

3.2.2 Experimental features on wetting-dewetting transition

The static CA features of the three varieties of the rose petals are shown in Figs. 4a–4c and Table 2. The shape of the water droplets at a base-tilting of 0° and 90° are depicted in Figs. 5a–5c and the curves representing advancing (max.) and receding (min.) CA with varying tilting angles as well as CA hysteresis traces can be found in Figs. 6a–6d. The petal surfaces are essentially hydrophobic with a maximal CA exhibited by the DP petals at a higher tilting angle. As can be noticed, the DP rose petals exhibited a superbly high CA and r_φ value owing to a comparatively low p/h ratio (Table 1 and Table 2). To be specific, in this case, r_φ=2.94 and φ= 0.46. Amongst all, the off pink, LP rose petals offered comparatively low values of wetting-dewetting parameters, with r_φ= 2.27

Table 2 Measured parameters related to dewetting phenomena witnessed in rose-petal surfaces

Sample	Bump density (1/10,000 μm^2)	Static CA (˚)	Roughness factor, r_φ	Solid-water fraction, φ	Advancing and receding, CA(˚)	Transitional roughness, r_t	CAH (˚)	Critical angles, α_1; α_2 (˚)	Surface energy (mJ·m^{-2})
White rose (W)	27	122.5 ± 0.2	2.74	0.37	137; 86	1.23	51 ± 0.31	18˚; –	49.8
Light pink rose (LP)	33	111.2 ± 0.2	2.27	0.32	117; 90	1.83	27 ± 0.27	29˚; 57˚	152.8; 264
Dark pink rose (DP)	24	133.3 ± 0.2	2.94	0.46	142; 83	1.15	59 ± 0.33	18˚; 39˚	13.1; 28.6

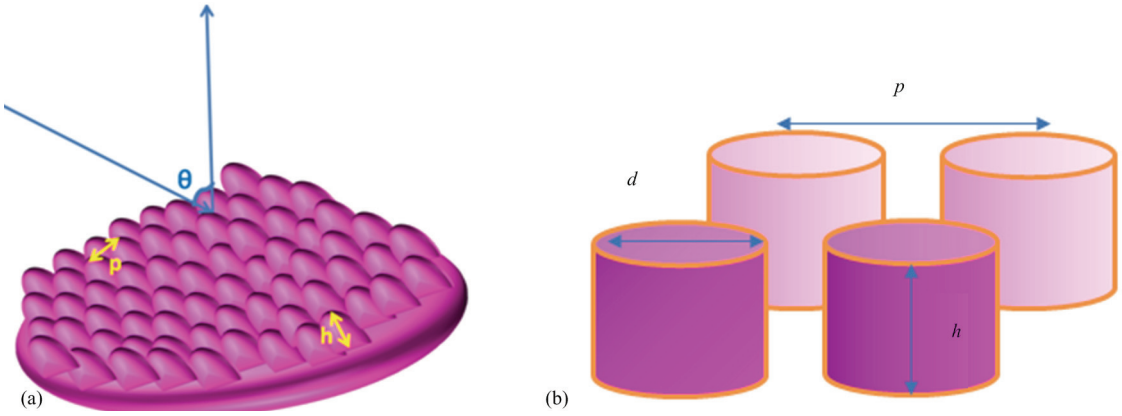

Fig. 3 (a) Schematic representation of an assembly of micro-papillae within a rose petal along with light scattering aspect and (b) side view of four micro-papillae in a square area highlighting pitch and height of the micro-papillae.

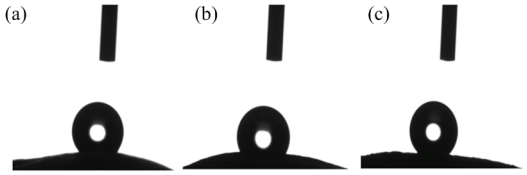

Fig. 4 Static water Contact Angle (CA) values measured on flat surfaces of (a) white (W), (b) light pink (LP), and (c) dark pink (DP) rose petals.

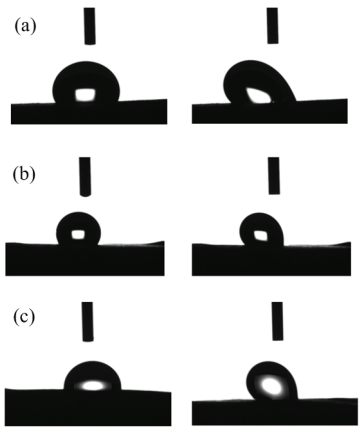

Fig. 5 The measured CA in tilting base methodology, with left and right columns representing views corresponding to a base tilting of 0˚ and 90˚; respectively. Note the advancing and receding surface contacts in the latter case. Here (a), (b), (c) represent characteristic features of W, LP, DP specimens; respectively.

and φ = 0.32. In fact, a higher value of the roughness factor is likely to improve surface hydrophobicity with marginal enhancement in the solid-water fraction as per Eq. (5). Apparently, an improved CA, high CAH and large r_φ values are mainly responsible for displaying enhanced hydrophobic feature. On the other hand, the water droplet may develop a tendency to impregnate into the grooves for a moderate rough surface. In contrast, a different correlation has been realized by us in insect systems, such as, damsel and dragonfly wings[30].

Wetting transition is an important mechanism which needs to be understood for the development of super-hydrophobic surfaces. Normally, a particular system has a single, Young's CA value, relevant for a genuinely smooth surface structure. But one could observe altered CA values due to a variation in the local geometrical construction between any two sites. It has been explained theoretically that, Gibbs energy of a system has multiple minima and a single global minimum. Each of the CA value corresponds to the metastable state of the system and the global equilibrium is given by the so-called most stable CA[25]. We have measured the advancing (max.) and receding (min.) CA for every unit degree of base-tilting, from 0˚ to 90˚

(Figs. 6a–6d). With tilting progression, certain critical angles (α) are defined at which the droplet tends to slide. The angle at which the first displacement of the contact line occurs and the angle for which both the uphill and downhill contact lines are displaced are termed as critical angles[31]. The critical tilt angles are predicted as, 18° for W rose; 29° and at 57° for the LP rose; and 18° and 39° for the DP rose petals. The parameters as regards, CAH, critical angle and surface energy can be found in Figs. 6a–6d and Table 2.

Here, we witnessed significant changes in advancing and receding angles, which are in consistency with the petal effect. Since the rose petals under study vary in surface structure, wetting-dewetting feature also changes as can be noticed by CA and CAH plots. The CAH essentially foretells the state of a liquid droplet, with small CAH representing the droplet in Cassie state. As the droplet is allowed to slide on a surface with the tilting angle varying from 0° – 90°, the localised roughness is at work which prevents the droplet from rolling/rapid sliding. For a water droplet in case of Wenzel state, normally the CAH value increases with increasing surface roughness[32]. In the C-B state, however, the CAH is largely influenced by the solid-liquid fraction. Noting that, the DP rose petals which exhibited high values of r_φ, φ and CAH; when the droplet undergoes sliding, it would certainly experience changes along smaller pockets in terms of roughness, causing changes in the shape and curvature of the droplet. This will definitely allow transition between Cassie and Wenzel states. As the drop bends, it will develop tendency to penetrate the empty space between papillae, thus increasing the difference between the CA maxima and minima. Revealing CAH along with static CA enhances our insight on the effect of microstructure on water-repelling surfaces. The CAH influences the pinning of the droplet, which does not allow the droplet to roll off and consequently, while retaining the hydrophobicity the droplet did not roll off the surface, even though the base tilting reached a maximal value of 90°. The pseudo super-hydrophobic nature of the rose petals and gecko feet has already been referred in literature. Despite hydrophobic nature of the surfaces, the droplets do not necessarily roll off owing to the pinning effect predicted in earlier works[33].

The Wenzel and C-B models can be simultaneously applied to reveal the transitional roughness (r_t) at the transitional point[34], given by:

$$r_t = \varphi - (1-\varphi)/\cos\theta_{\text{adv}}, \tag{6}$$

with θ_{adv} as the equilibrium CA. Note the extrapolated black dotted line drawn from the saturation part of the advancing CA curve towards y-axis. Whereas, the red dotted line gives the receding angle (Figs. 6a–6c). The values of the transition point in the three rose varieties are listed in Table 2. For $r_\varphi < r_t$, the droplet penetrates into the grooves, and thus in the Wenzel mode. Whereas, for $r_\varphi > r_t$, the droplet is said to be in the Cassie state. Accordingly, the water droplet in all the rose petals would ensure Cassie state. While undergoing transition from the Wenzel to the Cassie state[34], it is marked by significant changes in the advancing and receding CA, witnessed in all the three rose-cultivars.

3.3 Structural colouration in rose petals

A comparative analysis of structural colour has been performed with the help of reflectance responses and chromaticity diagrams.

3.3.1 Manifestation of reflectance features

The characteristic reflectance spectra of the three varieties of rose specimens, namely White (W), Light Pink (LP) and Dark Pink (DP) studied with and without chemical treatment, are depicted in Figs. 7a–7c. As for surface treatment, the matured petal specimens were dipped in three different liquids, namely ethanol (RI=1.36), propanol (RI=1.39) and glycerine (RI = 1.47). The idea behind the liquid adsorption was to alter the micro-morphological features by varying the RI of the environment, which could bring in significant changes in the reflectance spectra. Earlier, the appearance of colour was believed to be caused by the change in the RI of the building elements or through transient modification in its dimensions[12]. The specimens offered either similar or different reflectance curves in a particular range of wavelengths. Referring to W and LP petals, the former exhibited a steadily growing reflectance trend beyond 400 nm along with a broad peak observable at ~510 nm. Whereas, the LP specimen displays a distinct reflectance maximum located at ~455 nm and a dip at

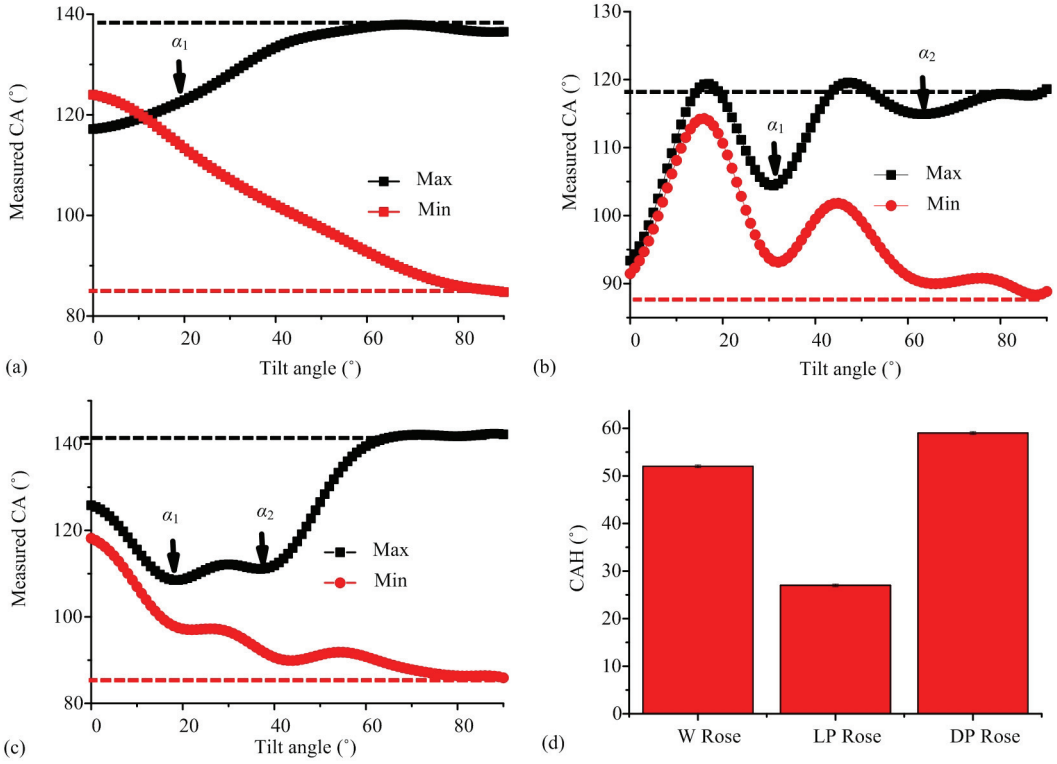

Fig. 6 Advancing (maximum) and receding (minimum) contact angles measured in tilting base methodology as for (a) white (W), (b) light pink (LP), and (c) dark pink (DP) rose petals. The histograms depicting CAH for the respective specimens are shown in (d).

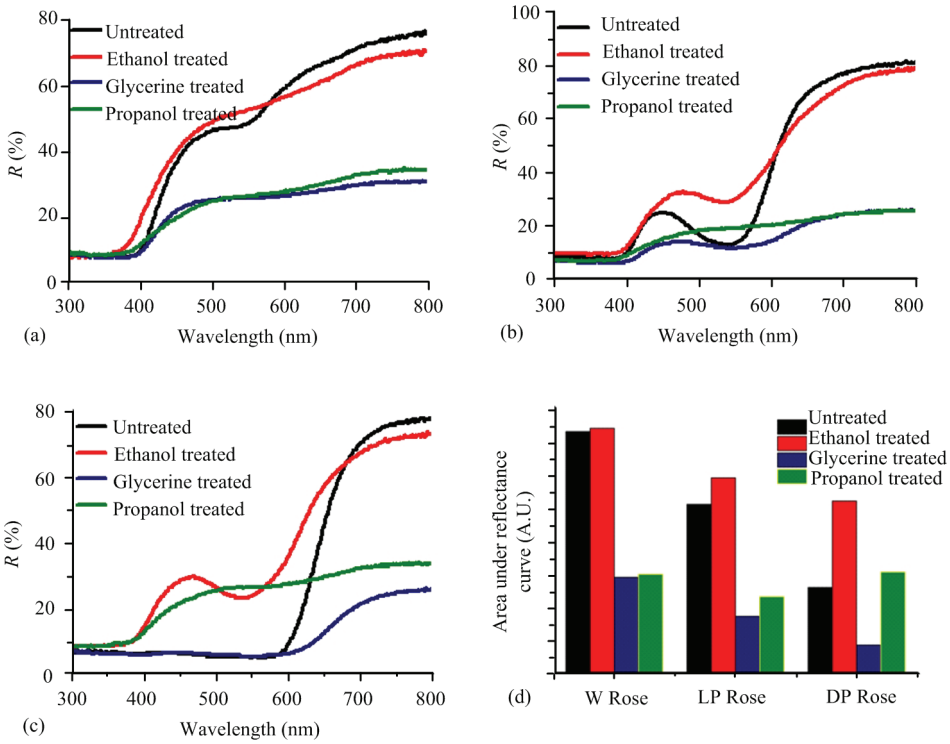

Fig. 7 Reflectance spectra of three varieties of *Rosaceae* cultivars before and after liquid immersion: (a) white (W), (b) light pink (LP), and (c) dark pink (DP) rose petals. The histograms highlighting comparative area under reflectance curves, before and after liquid immersions are depicted in (d).

~545 nm, beyond which reflectance feature showed a growing trend (Fig. 7b). On the other hand, the DP specimen has a poor reflectance up to ~590 nm, followed by a sharp rising trend afterwards. In other words, the petals of the dark pink rose would offer a dark impression to the unaided eyes, owing to intense light absorption in the visible wavelength range and excluding largely the orange-red part of the main electromagnetic spectrum. As can be noticed, the untreated specimen is highly reflective in the infrared regime (Fig.7c).

The insertion of these solvents with varying refractive indices into the air-pockets and sub-micron voids would change the *RI* of the petals as a whole. Note the modified reflectance curves (after liquid treatment) for W, LP and DP specimens (Figs. 8a–8d). Each of the soaked petals gave distinctly different characteristics with the emergence or disappearance of peak for a given specimen type. While ethanol dipped W rose petal, exhibited a similar, yet broadened reflectance feature in reference to the untreated one; propanol and glycerine treated W specimens provided significantly lowered reflectance features. Upon ethanol uptake, the LP rose petal gave a shifting of the reflectance peak from ~455 nm to 478 nm, however, the DP specimen offered the emergence of a new peak (located at ~465 nm), which was otherwise absent for the untreated case. As clearly seen from the reflectance curves of both LP and DP specimens, the colour tend to fade away for the specimens immersed in the liquids of propanol and glycerine. In these cases, we could also witness bleached view of the petals through the unaided eyes. It is interesting to note that, geraniol, a mono-terpenoid and alcohol, which constitutes an important component of rose oil, has *RI* = 1.46 in ambient environment. Most likely when voids are filled by glycerine, the whole specimen would behave as an entity dispersed with geraniol. As a result, structural contribution to colour is drastically suppressed and pigmentary contributions become more prominent (Fig. 8d). Thus one can say that, a substantial difference in *RI* within the treated petals can be set by ethanol and propanol media (Figs. 8b and 8c). To be specific, in case of ethanol treatment, one could realize a great similarity in the reflectance responses exhibited by the LP and DP petals. In contrast, after propanol uptake, all the specimens fade away and give similar trends. These aspects are ascribed to the momentary structural resemblance in the aforesaid petals. Consequently, they signify suppression/removal of the dyes.

Even though the colour that appears is a combinatorial effect of pigmentary and structural colour, the latter component gets altered once the *RI* of the environment is varied. Since the bands are generally broad, with reflectance responses between any two specimens different, we intended to focus on the LP petals, which exhibited a clear peak shifting upon chemical processing. A simple relationship between the optical stop bands and the periodicity of the nano-structured pattern can be given by the Bragg's law[1]:

$$\lambda = 2dn_{\text{eff}}, \tag{7}$$

$$\lambda' = 2dn'_{\text{eff}} = 2d(n_{\text{eff}} + \Delta n) = 2dn_{\text{eff}}[1 + \frac{\Delta n}{n_{\text{eff}}}], \tag{8}$$

where n_{eff} is the effective *RI* of the system under study and d is the period which is assumed to be unaltered before and after ethanol adsorption. The respective *RI* of the air gap, geraniol, ethanol, propanol and glycerine are approximately, 1.0, 1.46, 1.36, 1.39, 1.47. Consequently, the n_{eff} values can be 1.23, and 1.27, 1.28 and 1.31; as for the untreated, and specimens treated with ethanol, propanol and glycerine. Here, many ultra-small air pockets are still assumed to remain unfilled even after liquid adsorption. Inserting $\lambda = 455$ nm and $n_{\text{eff}} = 1.23$ in Eq. (7), we obtain d~185 nm. Apparently, this cannot be compared to the pitch of the micro-papillae which has micron scale dimension. However, the periodicity could be linked to the average repeat units of the nano-folders and air gaps that make up the micro-papillae. On substituting the values, d~185 nm and n_{eff} =1.27, 1.28 and 1.31 in Eq. (8), we obtain λ'~470 nm, 474 nm and 485 nm which can be witnessed in the corresponding reflectance curves, shown in Figs. 7 and 8. It is, however, worth mentioning that, while the strength of reflectance is largely described through the surface microstructure, the wavelength at which most of the light is reflected has its origin on the conditions set by specular and diffuse scattering events. Earlier, the peak maximum at a higher wavelength for the rose petals was ascribed to the contribution due to a mutual combination of structure and pigment[1].

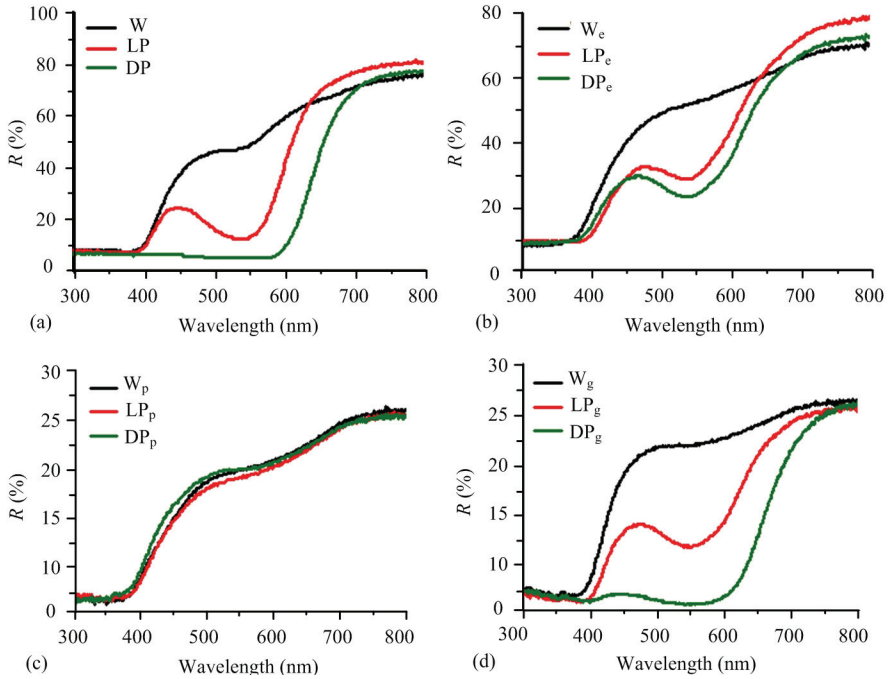

Fig. 8 Reflectance curves of rose petals without and with liquid immersions, shown collectively in (a) – (d).The respective labels W_e, LP_e and DP_e; W_p, LP_p and DP_p; W_g, LP_g and DP_g represent specimens after ethanol, propanol and glycerine treatment.

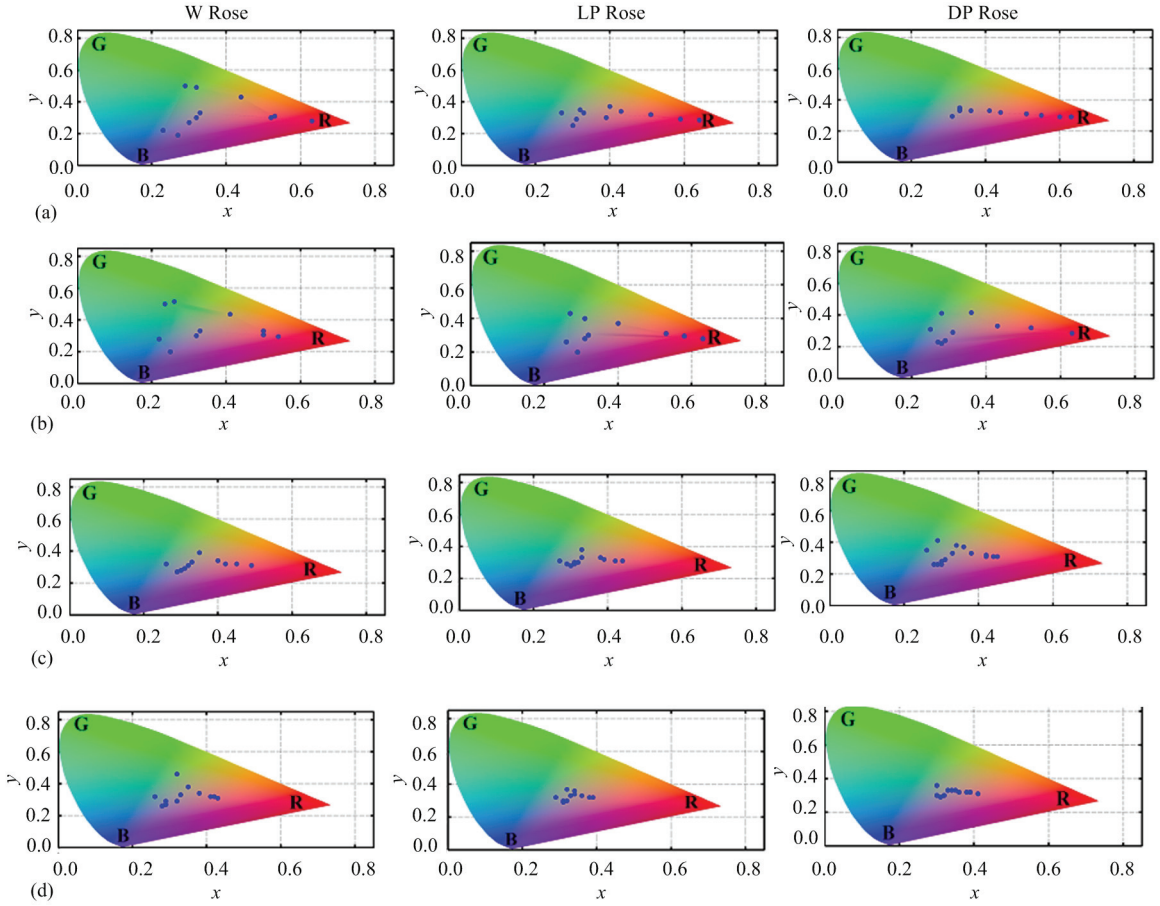

Fig. 9 CIE chromaticity diagrams corresponding to the untreated white (W), light pink (LP), and dark pink (DP) rose petals are shown in (a) (col. 1, 2 and 3). The chromaticity features as for the ethanol, propanol and glycerine treated specimens are presented in rows (b), (c) and (d); respectively.

3.3.2 Chromaticity features

We have also translated the reflectance data into chromaticity diagrams, employing CIE 1931 colour space[16]. Essentially, a chromatogram characterizes the loci of the wavelength reflected with different intensities, by converting the wavelength to the (x, y) coordinates, known as chromaticity coordinates. The chromaticity diagrams can be extremely useful as they are capable of identifying and assigning the exact colour of a given specimen in the colour space. Such diagrams are extremely meaningful for describing coloured species even for multi-coloured butterflies[35]. The diagrams for different rose petals can be found in Figs. 9a–9d. Here, an arbitrary point on the line joining between any two apex colours would represent a proportionate mixture of those. The triangular gamut formed as a result of the line joining B, G and R depends on the choice of focus with the centroid, identified as pure white (W^*). The white rose petals, without and with ethanol treatment, exhibited scattered points around W^* with slight stretching along terminus R (Figs. 9a, 9b, col.1). However, a more precise accumulation of points within the central region along with directed extension towards R has been clearly witnessed in the LP specimen (Fig. 9a, col.2). Upon ethanol treatment, the points representing reflectance response around the central region is much scattered without loss of generality with regard to the untreated case (Fig. 9b, col. 2). Not surprisingly, the DP rose specimen gave a continuous stretch of the reflectance points from around the vicinity of W^* to the R terminus (Fig. 9a, col.3). In other words, the dark appearance of DP specimen could be due to the dominance of R segment in the aligned gamut of the colour space. Upon ethanol uptake, the distribution of reflecting points of the LP specimen is more open at the centroid and the chromaticity pattern becomes quite similar as to the treated DP rose specimen (Fig. 9b, col. 2 and 3). At the microstructural level, both the LP and DP rose petals would share a common physical trend after the ethanol insertion. Accordingly, similar reflectance and chromaticity features have been ensured. This is, because, ethanol uptake is likely to cover up many of the rough surfaces by way of filling air pockets/voids available within and around the micro-papillae. The visible light would experience adequate surface scattering from the bumpy assembly of micro-papillae which essentially depends on varying p/h value. Moreover, a lowered bump density and pitch value in the DP petals offered a stronger absorption response and consequently, a deep pink colour appears to the unaided eye. Furthermore, the chromaticity diagrams, particularly for the propanol and glycerine treated specimens (Figs. 9c, 9d, col.2 and 3), exhibited apparent accumulation of points around the W*, thereby indicating colour fading in these cases as discussed above. In fact, propanol medium offered strongest discolouration effect while displaying similar reflectance features as well as colorigrams for all rose-specimens (Figs. 8c and 9c).

4 Conclusion

The cultivars of *Indian Rosaceae* family have been examined to exploit surface wettability and structural colouration characteristics. The surface roughness, r_φ which is highly dependent on the nature of arrangement of micro-papillae with different p/h ratio plays an important role for displaying de-wetting feature. With a lowered pitch-to-height ratio, the DP rose petal exhibited maximal values of static CA (= 133°), r_φ (= 2.94) and CAH (= 59°). As compared to the other two varieties, the reflectance response of DP specimen is significantly lowered over the whole visible wavelength range. However, immersion in ethanol, propanol and glycerine could facilitate distinct roles for improving reflectance feature. In particular, a prominent reflectance peak appeared after ethanolic uptake. Moreover, the reflectance features of the LP and DP specimens after ethanol-treatment are quite similar owing to the establishment of a common micro-morphological and optical trend. Similarly, propanol treatment gave quite alike reflectance features, for all cultivar-types. The dimension and distribution of the micro-papillae or micro-bumps, were believed to influence the surface morphology drastically. Connecting wettability with reflectance trend mediated *via* surface roughness characteristics would find scope in softonics by way of bridging soft matter physics and biophotonics at large. More work, in this direction is in progress for other natural systems.

Acknowledgment

The authors acknowledge DST-SERB, New Delhi

(EMR/2016/008045) for the grant and colleagues for their helpful suggestions. The authors also thank SAIC, TU for extending imaging facility using scanning electron microscopy.

References

[1] Feng L, Zhang Y, Li M, Zheng Y, Shen W, Jiang L. The structural color of red rose petals and their duplicates. *Langmuir*, 2010, **26**, 14885–14888.

[2] Glover B J, Whitney H M. Structural colour and iridescence in plants: The poorly studied relations of pigment colour. *Annals of Botany*, 2010, **105**, 505–511.

[3] Wang Z L, Guo Z G. Biomimetic photonic structures with tunable structural colours: From natural to biomimetic to applications. *Journal of Bionic Engineering*, 2018, **15**, 1–33.

[4] Vukusic P, Sambles J R. Photonic structures in biology. *Nature*, 2003, **424**, 852–855.

[5] Vukusic P, Sambles J R, Lawrence C R, Wootton R J. Structural colour: Now you see it – now you don't. *Nature*, 2001, **36**, 410.

[6] Vukusic P, Sambles J R, Lawrence C R. Structural colour: Colour mixing in wing scales of a butterfly. *Nature*, 2000, **404**, 457.

[7] Zi J, Yu X, Li Y, Hu X, Xu C, Wang X, Liu X, Fu R. Coloration strategies in peacock feathers. *Proceedings of the National Academy of Sciences*, 2003, **100**, 12576–12578.

[8] Parker A R, Welch V L, Driver D, Martini N. Structural colour: Opal analogue discovered in a weevil. *Nature*, 2003, **426**, 786–787.

[9] Parker A R, McPhedran R C, McKenzie D R, Botten L C, Nicorovici N A. Photonic engineering. Aphrodite's iridescence. *Nature*, 2001, **409**, 36–37.

[10] Kinoshita S, Yoshioka S. Structural colors in nature: The role of regularity and irregularity in the structure. *ChemPhysChem*, 2005, **6**, 1442–1459.

[11] Han Z W, Yang M, Li B, Mu Z, Niu S C, Zhang J Q, Yang X. Excellent color sensitivity of butterfly wing scales to liquid mediums. *Journal of Bionic Engineering*, 2016, **13**, 355–363.

[12] Whitney H M, Kolle M, Andrew P, Chittka L, Steiner U, Glover B J. Floral iridescence, produced by diffractive optics, acts as a cue for animal pollinators. *Science*, 2009, **323**, 130–133.

[13] Antoniou Kourounioti R L, Band L R, Fozard J A, Hampstead A, Lovrics A, Moyroud E, Vignolini S, King J R, Jensen O E, Glover B J. Buckling as an origin of ordered cuticular patterns in flower petals. *Journal of Royal Society Interface*, 2013, **10**, 20120847.

[14] Nosonovsky M, Bhushan B. *Green Tribology*, *Green Energy and Technology*, Springer-Verlag, Berlin, Heidelberg, Germany, 2012.

[15] Feng L, Zhang Y, Xi J, Zhu Y, Wang N, Xia F, Jiang L. Petal effect: A superhydrophobic state with high adhesive force. *Langmuir*, 2008, **24**, 4114–4119.

[16] Cambridge international examinations (CIE). In *Commission Internationale de l'Eclairage Proceedings*, Cambridge University Press, Cambridge, UK, 1931.

[17] Kinoshita S. *Structural Colors in the Realm of Nature*, World Scientific Publishing, Singapore, Singapore, 2008.

[18] Ebert D, Bhushan B. Wear-resistant rose-petal effect surfaces with superhydrophobicity and high droplet adhesion using hydrophobic and hydrophilic nanoparticles. *Journal of Colloid and Interface Science*, 2012, **384**, 182–188.

[19] Saito A. Material design and structural color inspired by biomimetic approach. *Science and Technology of Advanced Materials*, 2012, **12**, 064709.

[20] Image J, [2017-12-29], http://imagej.nih.gov/ij/

[21] Cassie A B D. Contact angles. *Discussions of the Faraday Society*, 1948, **3**, 11–16.

[22] Wenzel R N. Surface roughness and contact angle. *Journal of Physical Chemistry*, 1949, **53**, 1466–1467.

[23] Blossey R. Self-cleaning surfaces – Virtual realities. *Nature Materials*, 2003, **2**, 301–306.

[24] Bhushan B, Nosonovsky M. The rose petal effect and the modes of superhydrophobicity. *Philosophical Transactions of the Royal Society A*, 2010, **368**, 4713–4728.

[25] Pierce E, Carmona F J, Amirfazli A. Understanding of sliding and contact angle results in tilted plate experiments. *Colloids and Surfaces A*: *Physicochemical and Engineering Aspects*, 2008, **323**, 73–82.

[26] Nosonovsky M. Model for solid-liquid and solid-solid friction of rough surfaces with adhesion hysteresis. *Journal of Chemical Physics*, 2007, **126**, 224701.

[27] Bormashenko E, Stein T, Pogreb R, Aurbach D. Petal effect on surfaces based on Lycopodium: High-stick surfaces demonstrating high apparent contact angles. *Journal of Physical Chemistry C*, 2009, **113**, 5568–5572.

[28] Schulte A J, Droste D M, Koch K, Barthlott W. Hierarchically structured superhydrophobic flowers with low hysteresis of the wild pansy (Viola tricolor) – New design principles for biomimetic materials. *Beilstein Journal of Nanotechnology*, 2011, **2**, 228–236.

[29] Bhushan B, Chae J Y. Wetting study of patterned surfaces for superhydrophobicity. *Ultramicroscopy*, 2007, **107**, 1033–

1041.

[30] Aideo S N, Mohanta D. Limiting hydrophobic behavior and reflectance response of dragonfly and damselfly wings. *Applied Surface Science*, 2016, **387**, 609–616.

[31] White J A, Santos M J, Rodríguez-Valverde M A, Velasco S. Numerical study of the most stable contact angle of drops on tilted surfaces. *Langmuir*, 2015, **31**, 5326–5332.

[32] Kim D, Pugno N M, Ryu S, Wetting theory for small droplets on textured solid surfaces. *Scientific Reports*, 2016, **6**, 37813.

[33] Webb H K, Crawford R J, Ivanova E P. Wettability of natural superhydrophobic surfaces. *Advances in Colloid and Interface Science*, 2014, **210**, 58–64.

[34] Yeh K Y, Chen L J, Chang J Y. Contact angle hysteresis on regular pillar-like hydrophobic surfaces. *Langmuir*, 2008, **24**, 245–251.

[35] Aideo S N, Haloi R, Mohanta D. Exploring structural colour in uni- and multi-coloured butterfly wings and Ag^{+} uptake by scales. *Europhysics Letters*, 2017, **119**, 66003.